ACS APPLIED MATERIALS & INTERFACES

Research Article

www.acsami.org

Ultrasound, pH, and Magnetically Responsive Crown-Ether-Coated Core/Shell Nanoparticles as Drug Encapsulation and Release Systems

Siu-Fung Lee,[†] Xiao-Ming Zhu,[‡] Yi-Xiang J. Wang,[‡] Shou-Hu Xuan,[†] Qihua You,[§] Wing-Hong Chan,[§] Chi-Hin Wong,[§] Feng Wang,[†] Jimmy C. Yu,[†] Christopher H. K. Cheng,[⊥] and Ken Cham-Fai Leung*[,†,§,#,∥]

[†]Department of Chemistry, [‡]Department of Imaging and Interventional Radiology, Prince of Wales Hospital, [⊥]School of Biomedical Sciences, The Chinese University of Hong Kong, Shatin, NT, Hong Kong SAR, P. R. China

[§]Department of Chemistry and [#]Institute of Creativity, The Hong Kong Baptist University, Kowloon Tong, Kowloon, Hong Kong SAR, P. R. China

[∥]Institute of Molecular Functional Materials, University Grants Committee, Hong Kong SAR, P. R. China

Supporting Information

ABSTRACT: Core@shell nanoparticles with superparamagnetic iron oxide core, mesoporous silica shell, and crown ether periphery were fabricated toward drug delivery and tumor cell imaging. By the concept of nanovalve based on supramolecular gatekeeper, stimuli-responsive drug delivery nanosystems Fe_3O_4@SiO_2@meso-SiO_2@crown ethers were synthesized by (i) modified solvothermal reaction; (ii) sol−gel reaction; and (iii) amide coupling reaction. The successful coupling of the dibenzo-crown ethers onto the mesoporous silica shell was confirmed by thermogravimetric analysis and Infrared spectroscopy. In this system, the "ON/OFF" switching of the gatekeeper supramolecules can be controlled by pH-sensitive intramolecular hydrogen bonding or electrostatic interaction (such as metal chelating). Biological evaluation of the nanoparticles renders them noncytotoxic and can be uptaken by L929 cells. In this work, the antitumor drug (doxorubicin) loading and release profiles which were studied by the UV/visible absorption spectroscopy. The mechanism involves the best-fit binding of crown ethers with cesium or sodium ions at different pH values with ultrasonic wave in phosphate buffered saline (PBS). Magnetic resonance imaging analysis of the particles reveals a high relaxivity, rendering them potentially useful theranostic agents.

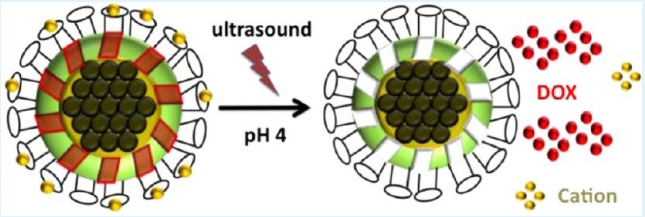

KEYWORDS: *crown ether, drug carrier, magnetic resonance imaging, nanoparticle, ultrasound*

1. INTRODUCTION

Multifunctional hybrid nanostructured materials comprising inorganic porous core nanostructures and organic shells have been widely developed for imaging, targeting, and drug delivery. These materials have been designed to release the drug payload at a specific lesion site with a suitable dosage over a period of time.[1−10] Recent investigation of noninvasive hyperthermia drug release from superparamagnetic iron oxide (SPIO)-based nanostructures has been explored by using alternating magnetic field.[11] However, the use of noninvasive ultrasound for releasing drug payloads from SPIO-based structures for multifunctional theranostic purposes has been less studied.[12,13] Ultrasound is a physical stimulus composed of acoustic waves that can exert localized effects on target sites. The cellular changes associated with ultrasound application include changes in the permeability of the cell membrane and in the transport of ions and molecules across this membrane. Application of ultrasound transiently permeabilizes cell membranes and offers a nonchemical, nonviral, and noninvasive method for cellular drug delivery with nanoparticles (NPs). It plays an important role for ultrasound-sensitive nanoparticles as contrast agents for ultrasound molecular imaging and for improved delivery of chemotheraprutic drugs and gene therapies across biological barriers, enabling a monitor of treatment responses and guiding therapies.[14−20] Ultrasound irradiation could generate reactive oxygen species from titanium dioxide nanoparticles for sonodynamic therapy.[21,22] Clinical ultrasound instruments are widely employed for real-time infant diagnosis of pregnant women thereby would not cause harmful effect to them.

With the concept of nanovalve-gatekeeper system of porous nanoparticles,[23,24] we report herein doxorubicin-carrying porous SPIO nanoparticle systems decorated with a series of crown ether macrocycles[25] for controlled release with ultrasound waves. The cytotoxicity, magnetic resonance response, systematic drug release profiles at two different pH environments, and mechanism postulation of these nanoparticle systems have been evaluated and discussed. pH-Dependent and controlled drug release from nanoparticles at a situation that can mimic the cell's endosome/lysosome (pH ∼4−5.5)

Received: July 13, 2012
Accepted: February 7, 2013
Published: February 12, 2013

   dx.doi.org/10.1021/am4004705 | ACS Appl. Mater. Interfaces 2013, 5, 1566−1574

environment would be promising for cancer theranostic applications.[26]

2. EXPERIMENTAL SECTION

Preparation of Fe_3O_4@SiO_2@meso-SiO_2@crown ether Nanoparticles. The dried **Fe_3O_4@SiO_2@meso(CTAB)-SiO_2-NH_2** NP (30 mg) was dispersed in dry DMF (50 mL) under a nitrogen atmosphere. *N*-Hydroxysuccinimide (NHS) (44.8 mg), dibenzo-crown ethers **1a**/**1b**/**1c** (**1a**−**c**), and *N*,*N*′-dicyclohexylcarbodiimide (DCC) (79.1 mg) were dissolved in dry DMF (30 mL), and then added into the solution slowly under ultrasonication. After an hour, the reaction was performed under mechanical stirring under nitrogen at 30 °C for 48 h. The product was collected by the help of magnet and then washed with DMF, ethanol, and water successively several times, to remove excess dibenzo-crown ethers, NHS, DCC, and surfactant (CTAB). Finally, the product was dried under reduced pressure for 12 h to obtain desired **Fe_3O_4@SiO_2@meso-SiO_2@crown ethers(1a-c)** NPs.

Cytotoxicity Study. A number of 10 000 L929 cells were seeded into the wells of a 96-well plate. After an incubation of 12 h, the culture medium in the wells was replaced by DMEM (10% FBS, 90 μL). Then, serial dilutions of NPs (10 μL) were added to give final iron concentrations ranging from 6.25 to 100 μg Fe/mL. After an incubation for 24 h, the MTT protocol of cytotoxicity study was performed.

MTT Protocol. MTT solution (5 mg/mL, 10 μL) was added to each well. After an incubation for 4 h, the culture medium was removed and formazan crystals were dissolved with 150 μL DMSO for 10 min on a shaker. The absorbance of each well was measured by a microplate reader at the wavelength of 540 nm. The relative cell viability (%) for each sample related to control well was calculated.

Cell Adhesion Study. A number of 10 000 L929 cells were seeded into each well of a 96-well plate. After an incubation of 12 h, the medium in the wells was replaced by DMEM (10% FBS for L929, 90 μL). Then, 10 μL serial dilutions of NPs were added to give final iron concentrations ranging from 6.25 to 100 μg Fe/mL. After an incubation for 4 h, the MTT protocol of cytotoxicity study was performed.

Cell Proliferation Study. A number of 5,000 L929 cells were seeded into each well of a 96-well plate. After an incubation for 12 h, the culture medium in the wells was replaced with DMEM (10% FBS for L929, 90 μL). Then, 10 μL serial dilutions of NPs were added to give final iron concentrations ranging from 6.25 to 100 μg Fe/mL. After incubation for 24, 48, or 72 h, the MTT protocols were performed respectively.

Cellular Uptake of Functionalized Nanoparticles. The cellular uptake of **Fe_3O_4@SiO_2@meso-SiO_2-NH_2 and Fe_3O_4@SiO_2@meso-SiO_2@crown ether(1a-c)** NPs were evaluated in L929, HepG2, and HT29 cells by Prussian blue staining. In addition, intracellular iron concentration study of L929 was evaluated by ICP-OES. The cells were seeded in a 24-well plate in DMEM medium containing 10% FBS. After an incubation for 12 h, the culture medium was replaced with serum-free DMEM medium containing NPs with the concentration of 5 μg Fe/mL and incubated for another 20 h. At the end of incubation, cells were washed with PBS 3 times, and Prussian blue staining or ICP-OES analysis was performed. In Prussian blue staining, cells were fixed for 40 min by using 4% paraformaldehyde. After washing with PBS, the cells were incubated with Perls' reagent (4% potassium ferrocyanide and 6% HCl) for 30 min, and followed by a neutral red counterstain. The cells were observed using a light microscopy. To determine intracellular iron concentration, the cells were collected and counted. Cells were resuspended in 200 μL of 12% HCl solution and incubated at 60 °C for 4 h to dissolve the NPs. Few drops of concentrated aqueous $SnCl_2$ were added, and the solution was further diluted to 1 mL. Subsequently, ICP-OES was performed to study the iron concentration of the residue.

Drug Loading of Functionalized Nanoparticles. The NP solution (1 mg/mL, 200 μL), DOX solutions (1 mg/mL, 100 μL) and stimuli (100 μL, 1 M NaCl, 1 M CsCl, PBS, 0.1 M HCl, or deionized H_2O) were mixed. The drug loading was performed for 24 h. Then, magnetic NPs were separated under the help of magnet and 200 μL of mixture was withdrawn for the UV/Visible absorption spectroscopic measurement (from 200 to 800 nm), such that the drug loading efficiency under different stimulus can be evaluated.

Drug Release of Functionalized Nanoparticles. The NP solution (1 mg/mL, 1 mL) was loaded with DOX (2 mg/mL, 0.5 mL) in deionized H_2O. The loading efficiency was determined by UV/Visible absorption spectroscopy. The pore entry of NPs was blocked by addition of 500 μL of capping agent (0.1 M HCl, 1 M CsCl, or 1 M NaCl) and followed by washing with capping agent three times (500 μL x 3). The loading efficiency of NPs after washing was then determined by separation of NPs with the help of magnet. Drug release upon ultrasound application was facilitated by using Sonics VCX130 (20 kHz, 130 W and 50% power intensity). The release profile of NPs was performed in PBS (at different pH) and monitored by UV/visible absorption spectroscopy. For drug release studies with ultrasound, data were collected by sonication of NPs for 5 min, followed by 3 min of separation under magnetic field.

MRI Study of Nanoparticles. Two NPs samples were dispersed in deionized H_2O at iron concentrations ranging from 0.3 to 5 μg Fe/mL. For MR measurements, dispersed NPs solutions at different concentrations were filled separately in Eppendorf tubes (1.5 mL). T_2 relaxation times were measured using a standard Carr-Purcell-Meiboom-Gill pulse sequence [time of repetition (TR) = 2000 ms, time of echo (TE) range = 30−960 ms, 32 echoes, field of view (FOV) = 134 × 67 mm^2, matrix = 128 × 64, slice thickness = 5 mm, NEX = 3]. T_2 relaxation times were calculated by a linear fit of the logarithmic ROI signal amplitudes versus TE. The T_2 relaxivities (r_2) were determined by a linear fit of the inverse relaxation times as a function of the iron concentrations used.

3. RESULTS AND DISCUSSION

Core@shell **Fe_3O_4@SiO_2@meso-SiO_2** and **Fe_3O_4@SiO_2@meso(CTAB)-SiO_2-NH_2** NPs were prepared by modified hydrothermal and sol−gel reactions.[27−29] The first SiO_2 layer acts as a template for a second SiO_2 coating with mesopores. A series of dibenzo-crown ethers was designed to act as the gatekeepers of nanovalves with the aim for NP-based drug delivery. Novel dibenzo-crown ethers **1a**−**c** (Figure 1) which consist of two carboxylic groups, could be synthesized (see Scheme S1 in the Supporting Information) and coupled to the amine surface of a hexagonal pore of mesoporous silica NPs, forming amide linkages. Also, preorganized crown ethers possess electrostatic interactions toward different cations, allowing the possibility of using different metal ions act as a capping agent. In this nanosystem, dibenzo-crown ethers were coupled onto the pores entry of the NPs to control the release of substrates. The capping agent can be either metal ions or simply a proton.[30] In the presence of capping agent, drug molecules would not be diffused freely, and escaped from the pores of NPs. However, it is expected that the effectiveness of hydrogen bonded supramolecular capping agents and then the release of drug molecules from the pores of NPs can be triggered by ultrasonic waves.[31−35] Moreover, ultrasonic devices with tunable energy intensities could be clinically available and that they are routinely used for noninvasive prenatal diagnosis. Also, the capping agent (Na^+ or H^+) is used in the nanovalves to mimic the environments of blood and slightly acidic (pH ∼4−5.5) cancer lesion site.[24,26] Therefore, the leakage of drug from the NPs in the body can be minimized because of the dissolution of capping agent before cellular uptake.

Mesoporous **Fe_3O_4@SiO_2@meso(CTAB)-SiO_2-NH_2** NPs underwent coupling reactions with dibenzo-crown ethers **1a**−**c** in the presence of NHS and DCC and followed by CTAB removal, yielding the desired NPs **Fe_3O_4@SiO_2@meso-SiO_2@**

dx.doi.org/10.1021/am4004705 | ACS Appl. Mater. Interfaces 2013, 5, 1566−1574

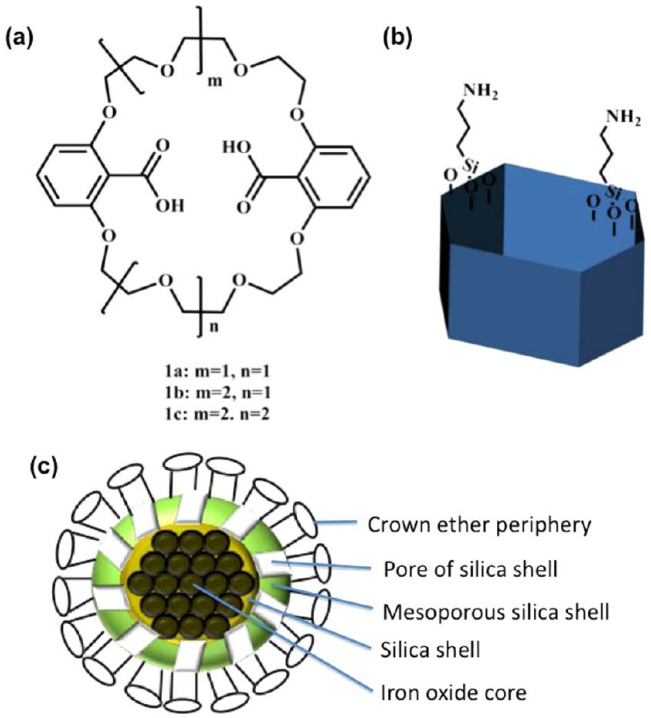

Figure 1. (a) Structural formula of the novel dibenzo-crown ethers **1a–c**; (b) schematic diagram of a hexagonal pore of amine-functionalized mesoporous silica NP; and (c) schematic diagram of a **Fe_3O_4@SiO_2@meso-SiO_2@crown ether** core@shell nanoparticle.

crown ethers(1a-c) by magnetic separation. From the TEM images (Figure 2), the core@shell nanostructures with an average diameter of 250 nm had not jeopardized by the coupling and surfactant removal reactions. The mesopores of the silica shell layer can be clearly observed in their magnified TEM images (Figure 2a, c, e). The success of coupling between the dibenzo-crown ethers **1a–c** and **Fe_3O_4@SiO_2@meso-(CTAB)-SiO_2-NH_2** NPs is proven by IR spectroscopic characterization, confirming the presence of IR absorptions corresponding to N–H stretching, C=O stretching, and N–H bending. However, in the case of surface functionalization of NPs, the signal of the corresponding stretching or bending is significantly weakened. As observed in the FTIR spectrum shown in Figure 3, the N–H stretching and N–H bending are observed in all cases with different intensities, indicating that N–H bond is present either in amine group or amide group. To distinguish the amide and amine, the presence of C=O stretching is an important evidence. In the cases of dibenzo-crown ethers, C=O stretching at 1628 cm^{-1} is observed and the relative ratio compared to the N–H bending at 1548 cm^{-1} is increased. On the basis of this observation, it is reasonable to believe that the coupling between the dibenzo-crown ethers and the amine-functionalized NPs was successful.

Thermogravimetric analysis (TGA) provides the information on changes in weight of NPs with increasing temperature. It gives evidence of the % organic fraction in the samples. The TGA spectra of the functionalized mesoporous NPs are shown in Figure S14 in the Supporting Information. In the TGA spectra, two major weight loss events in the temperature range of 150 to 400 °C and 450 to 800 °C are observed. According to the literature,[36] the weight loss at 150 to 400 °C is corresponding to the thermal decomposition of NPs' surface organic moiety and/or surfactant molecules, while the weight loss at 450 to 800 °C is due to dehydroxylation of the silicate networks on mesoporous silica materials. Hence, the differences between the weight losses at 150 to 450 °C were important indication for the changes in functionality of the mesoporous silica shell. As shown in the spectra, the percentage weight loss after coupling with dibenzo-crown ethers **1a–c** is ranging from 7.7–7.9%, whereas the percentage weight loss before coupling is only 5.6%. From this result, 2% more of organic fractions were found after the crown ether coupling reaction and removal of surfactant molecules. Therefore, this result indicated that the coupling of dibenzo-crown ethers **1a–c** to the amine-functionalized NPs (**Fe_3O_4@SiO_2@meso(CTAB)-SiO_2-NH_2**) were successful. When an organic molecular layer (crown ethers with thickness about a few nm) is attached onto the nanoparticle having an average 200 nm in diameter, 2% weight of organic fraction is considered as effective coupling.

Nitrogen adsorption/desorption isotherms were performed for determining the specific surface areas and pore sizes of **Fe_3O_4@SiO_2@meso-SiO_2-NH_2** NPs with Barrett–Joyner–Halenda (BJH) method. The pore size distribution curve of these NPs (Figure 4) indicates that a layer of mesoporous coating with average diameter of 3.2 nm pores was obtained. Also, the BET surface area of NPs was determined as 405 ± 1 m^2/g. The relatively large surface area provided a high storage capacity for drug encapsulation in biomedical application. After coatings with organic molecules onto porous nanoparticles, the pore diameter and surface area of nanoparticle would not change significantly. Examples are pyrene[37] and oligo-(phenylene butadiynylene).[38] However, smaller nanoparticle perturbation on the pheriphery of the porous particle will affect greatly the pore size.[39]

To aim as drug delivery systems, biocompatibility of the NPs were evaluated.[40] In principle, NPs, which act as drug delivery carrier, must be noncytotoxic and can be preliminary estimated by determining its cytotoxicity through (3-(4,5-dimethylthiazol-2-yl)-2,5-diphenyltetrazolium bromide (MTT) assay. For MTT assays, the relative cell viabilities (%) for NPs related to control well toward L929 normal cells (a murine aneuploid fibrosarcoma cell line) were determined and shown in Figure 5. In all cases, the viability of L929 cells was not affected by exposure to various concentrations (12.5 to 100 μg Fe/mL) of NPs for 24 h. These results suggest that the four different NPs did not possess acute toxicity in L929 cells.

The effects of NPs on cell proliferation and cell growth for L929 cells were determined. Similarly, the effect was estimated by MTT essay and the results of cell proliferation study toward NPs are shown in Figure 5. High cell viability % represents that the NPs did not show any significant inhibition toward cell growth. For the cases of **Fe_3O_4@SiO_2@meso-SiO_2-NH_2**, **Fe_3O_4@SiO_2@meso-SiO_2@crown ether(1b)** and **Fe_3O_4@SiO_2@meso-SiO_2@crown ether(1c)** NPs, they do not show any effect on L929 cell proliferation at low concentrations (12.5 to 50 μg Fe/mL), whereas slight inhibition on cell proliferation after 72 h incubation was found at 100 μg Fe/mL. However, there was a slightly inhibition on cell proliferation toward L929 cell by **Fe_3O_4@SiO_2@meso-SiO_2@crown ether(1a)** NPs even at lower concentration after 72 h incubation. Hence, it is more likely that **Fe_3O_4@SiO_2@meso-SiO_2@crown ether(1a)** NPs were less biocompatible toward L929 cell when compared with other NPs.

In qualitative and quantitative analyses, cellular uptake of any Fe_3O_4-based NPs can be determined by inductively coupled plasma-optical emission spectroscopy (ICP-OES), by measur-

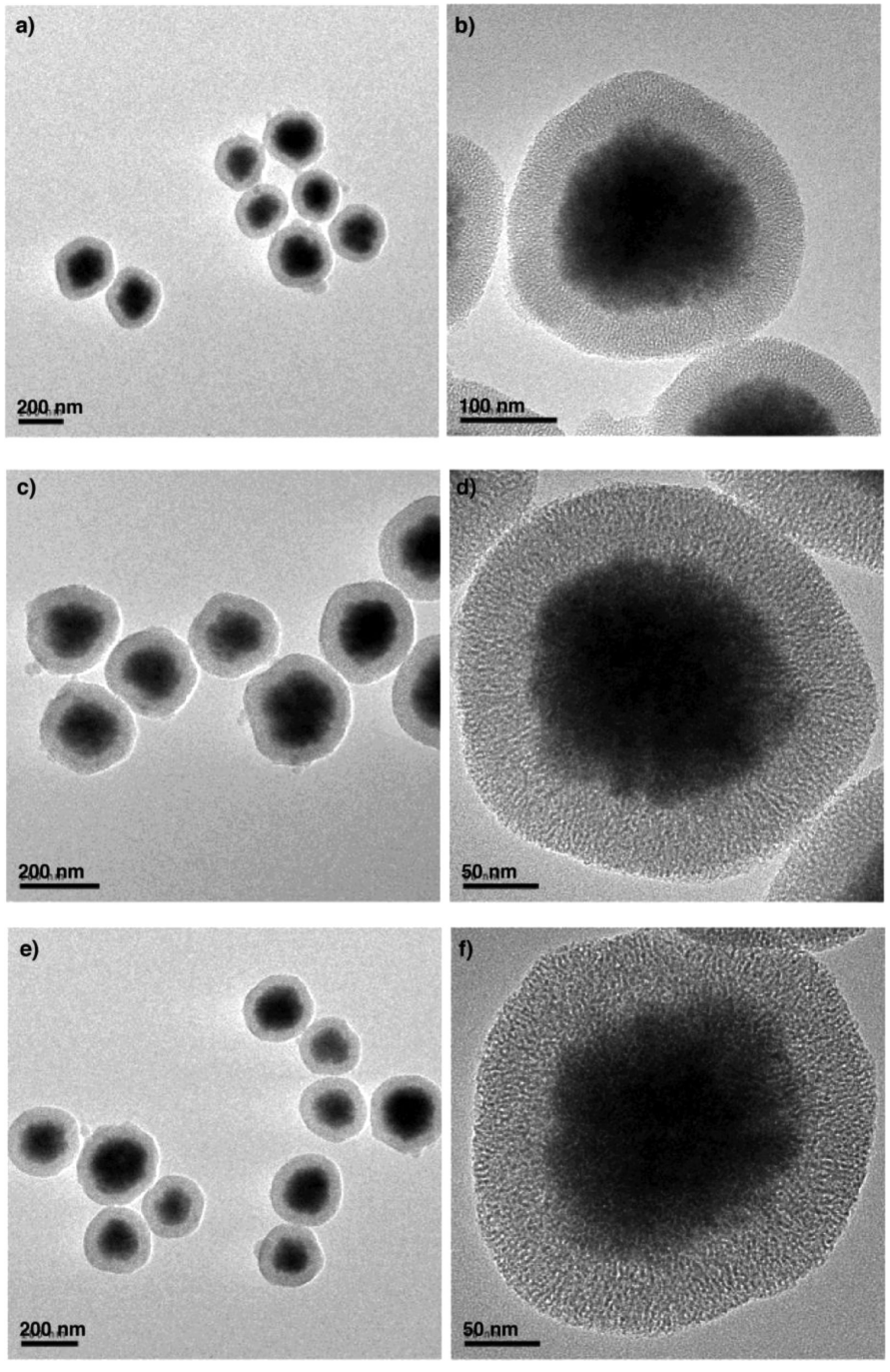

Figure 2. TEM images of the (a, b) Fe_3O_4@SiO_2@meso-SiO_2@crown ether(1a), (c, d) Fe_3O_4@SiO_2@meso-SiO_2@crown ether(1b), and (e, f) Fe_3O_4@SiO_2@meso-SiO_2@crown ether(1c).

ing the Fe content absorbed per cell, and Prussian blue staining method, to identify the presence of Fe by forming insoluble and highly colored complex. As shown in Figure 6, the images, which were obtained by Prussian blue staining method, indicated that NPs were absorbed into the L929 cell. Moreover, ICP-OES measurements were performed to determine the amount of Fe absorbed per cell. The amount of **Fe_3O_4@SiO_2@meso-SiO_2@crown ether(1a)**, **Fe_3O_4@SiO_2@meso-SiO_2@crown ether(1b)** and **Fe_3O_4@SiO_2@meso-SiO_2@crown ether(1c)** NPs absorbed per cell were determined to be 2.147×10^{-5}, 1.677×10^{-5}, and 2.295×10^{-5} μg/cell, respectively.

To act as a drug carrier, the drug-loading capabilities of NPs using different stimuli, such as pH, and selective metal ions, were investigated and monitored by UV/vis absorption spectroscopy. The drug loading processes involve the ON/OFF switching of nanovalves, i.e., the open and close of the nanopores by crown ethers. Prior to control the release of drug molecules from the nanoparticles, extensive washing processes were performed to ensured that no drug molecules were physically absorbed on top of the nanoparticles but were trapped inside the pores. Anticancer drug doxorubicin hydrochloric salt (DOX, 250 μg/mL) was used, which was monitored by the local maximum absorption wavelength at 480 nm.[41] The absorption spectra before and after drug loading of NPs for 24

dx.doi.org/10.1021/am4004705 | ACS Appl. Mater. Interfaces 2013, 5, 1566−1574

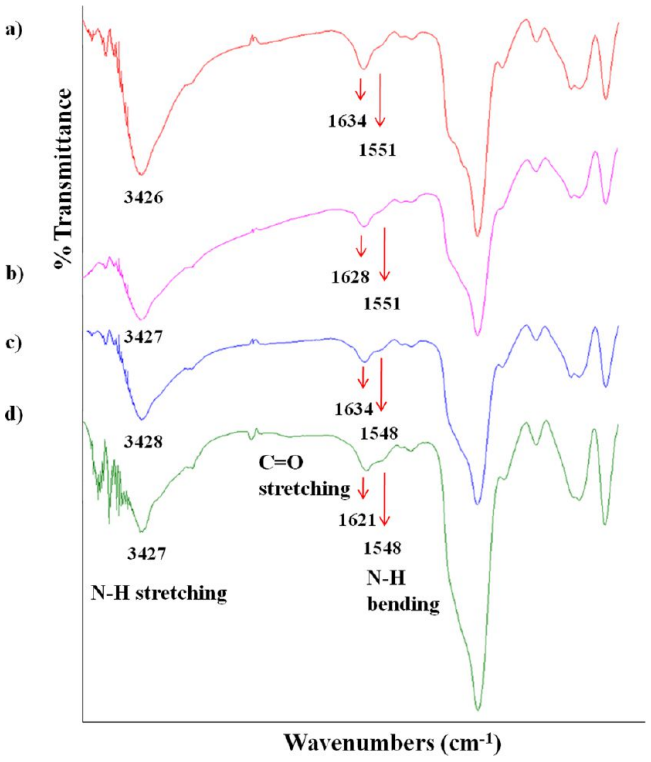

Figure 3. FTIR spectra of functionalized NPs, (a) Fe_3O_4@SiO_2@meso-SiO_2@crown ether(1a), (b) Fe_3O_4@SiO_2@meso-SiO_2@crown ether(1b), (c) Fe_3O_4@SiO_2@meso-SiO_2@crown ether(1c), and (d) Fe_3O_4@SiO_2@meso-SiO_2–NH_2.

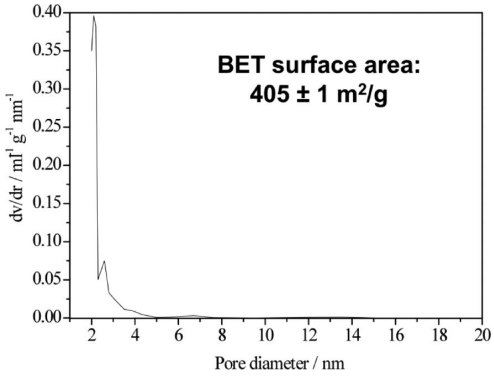

Figure 4. Pore size distribution curve of **Fe_3O_4@SiO_2@meso-SiO_2-NH_2** NPs.

h at pH 1 (with HCl) and pH 7 (H_2O) were obtained (see Figures S15–17 in the Supporting Information). Table 1 summarizes the % DOX drug loadings of different crown ether-coated NPs under different conditions. We employed **Fe_3O_4@SiO_2@meso-SiO_2-NH_2** nanoparticles as a control to compare the drug-loading % with the crown ether-coated nanoparticles. Although we believe that the **Fe_3O_4@SiO_2@meso-SiO_2-NH_2** nanoparticle would likely exhibit a different mechanism for drug loading and release based on the NH_2 groups augmented with electrostatic interactions, it is by far the simplest control model that we can obtain for investigation (the **Fe_3O_4@SiO_2@meso-SiO_2** nanoparticle also contains SiOH groups which would affect the drug loading and release mechanism). From Table 1, DOX drug loading of NPs can be facilitated in water with 47–55% loading. It indicates that at pH 1 with HCl, only 2–9% of DOX drug molecules were loaded to the **Fe_3O_4@SiO_2@meso-SiO_2@crown ether(1a-c)** NPs. 1–16% and 18–32% of DOX drug loadings were facilitated with CsCl and NaCl solutions, respectively. That is, the nanogates of **Fe_3O_4@SiO_2@meso-SiO_2@crown ether(1a-c)** are more tightly closed in acidic medium, Cs^+, or Na^+ when compared to pure water. In these conditions, therefore, the leakage of drug during the washing process will be significantly minimized, and the efficiency of drug storage will be higher. On the other hand, it suggests that the molecular crown ether gates is "open" as "ON" state at pH 7, and "close" as "OFF" state in acidic medium (H^+), Cs^+, or Na^+. It is reasonable to imply that the positively charged perturbating species H^+, Cs^+, or Na^+ would interact with the oxygen-rich, electronic donating crown ether's ethylene glycol chains to facilitate a blocking mechanism at the NP's pore for drug encapsulation.[42] The blocking effect of the NP's pore was influenced by the size matching between the sizes of cations and crown ether.

To act as an ideal drug delivery system, a controlled release of drug from NPs could be triggered immediately by the addition of stimuli. In our nanosystems, Cs^+ and Na^+ cations act as blocking agent for DOX drug-loaded NPs. Also, PBS with wither pH 4 or 7.4 were chosen for controlled drug release medium in order to obtain a better mimicking nanosystem toward biomedical applications. For the drug release profiles, the effect of blocking cations and dibenzo-crown ethers upon pH changes and ultrasound were studied. Cancer cell environment generally possesses a lower pH value than normal tissues. The changes in pH may lead to variation in electrostatic interaction and hydrogen bonding, whereas the gain of energy form ultrasound may lead to the dissociation of blocking agents from dibenzo-crown ethers. In addition, for the studies of ultrasound effect, each data was collected from every 5 min of sonication and followed by 3 min of magnetic separation. In Figure 6, drug release profiles of different crown ether-coated NPs with Cs^+ or Na^+ at two different pH values are shown. For the cases of **Fe_3O_4@SiO_2@meso(DOX)-SiO_2@crown ether-(1a)⊃M^+** NPs (Figure 7A), the DOX release at pH 4 from the **Fe_3O_4@SiO_2@meso(DOX)-SiO_2@crown ether(1a)⊃Na^+** NPs gave a controlled release with ultrasound with approximately 3-fold enhancement of the release (18%) over other systems (4–6%) using the same crown ether **1a**. The rate of DOX release was high for the first 10 min after a trigger with ultrasound. For the cases of **Fe_3O_4@SiO_2@meso(DOX)-SiO_2@crown ether(1b)⊃M^+** NPs (Figure 7B), the DOX release at pH 4 from the **Fe_3O_4@SiO_2@meso(DOX)-SiO_2@crown ether(1b)⊃Na^+** NPs gave a significant, controlled release with ultrasound with approximately 5-fold enhancement of the release (27%) over other systems at pH 7.4 (5–6%) using the same crown ether **1b**. However, **Fe_3O_4@SiO_2@meso(DOX)-SiO_2@crown ether(1b)⊃Cs^+** shows a continual leakage of DOX molecules over time but a slight release triggered by ultrasound. For the cases of **Fe_3O_4@SiO_2@meso(DOX)-SiO_2@crown ether(1c)⊃M^+** NPs (Figure 7C), the DOX release at pH 4 from the **Fe_3O_4@SiO_2@meso-(DOX)-SiO_2@crown ether(1c)⊃Na^+** NPs gave a substantial, controlled release with ultrasound (22%), whereas other systems show leakage of DOX molecules over time. The results demonstrated that the release of DOX drug from these NP systems can be influenced by pH and metal cations, thereby triggered by ultrasound application. Overall, there are very minimal "premature zero release" for the cases of **Fe_3O_4@SiO_2@meso(DOX)-SiO_2@crown ether(1a)⊃M^+** NPs (Figure 7A). This is a novel characteristic of our study. It is observed

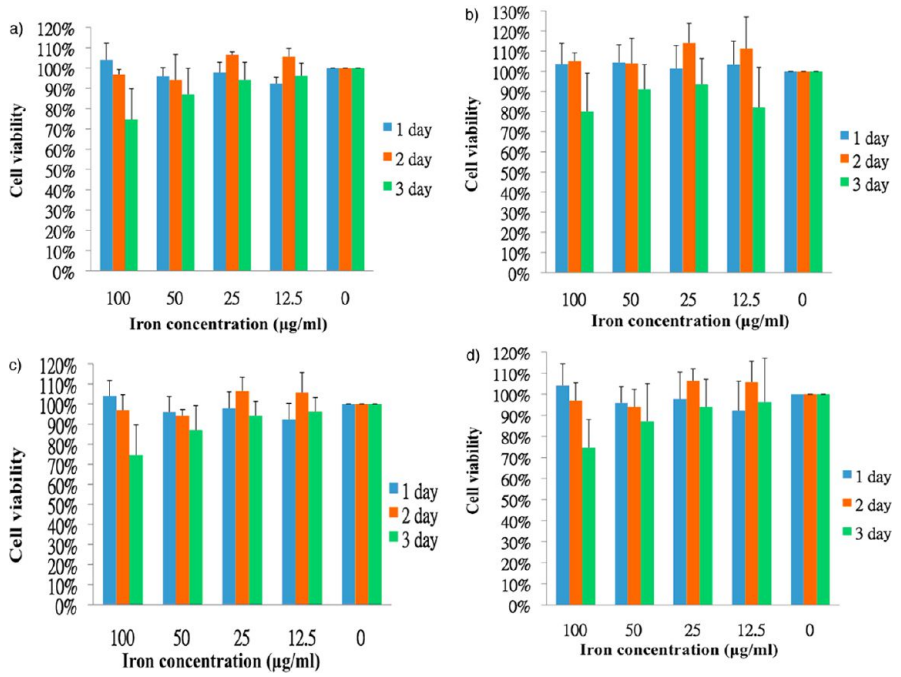

Figure 5. Viability of L929 cells exposed to (a) Fe_3O_4@SiO_2@meso-SiO_2@NH_2, (b) Fe_3O_4@SiO_2@meso-SiO_2@crown ether(1a), (c) Fe_3O_4@SiO_2@meso-SiO_2@crown ether(1b), and (d) Fe_3O_4@SiO_2@meso-SiO_2@crown ether(1c) NPs at various iron concentrations.

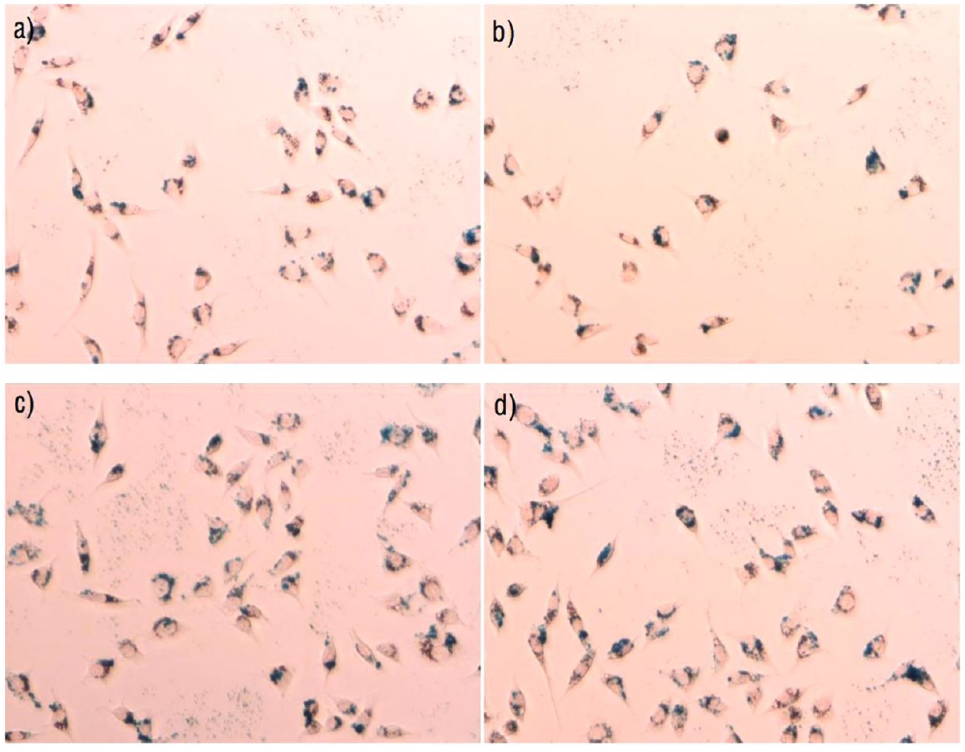

Figure 6. Cellular uptake of NPs at 5 μg Fe/mL toward L929 cell, with Prussian blue staining, (a) Fe_3O_4@SiO_2@meso-SiO_2@crown ether(1a), (b) Fe_3O_4@SiO_2@meso-SiO_2@crown ether(1b), (c) Fe_3O_4@SiO_2@meso-SiO_2@crown ether(1c), and (d) Fe_3O_4@SiO_2@meso-SiO_2–NH_2.

that crown ether **1b** and **1c**-coated nanoparticles are having premature zero release. There is a requirement when dealing with targeted drug delivery, to avoid that the toxic chemotherapeutic agents also reach healthy cells or tissues and therefore provoke undesired side-effects. Eventually, magnetic field can be used to guide the particles to the targeted specific lesion site (magnetic targeting).

The release profiles of DOX-loaded **Fe_3O_4@SiO_2@meso-SiO_2@NH_2** NPs have also been studied (see Figure S18 in the Supporting Information). Under the same conditions, with ultrasound application, only minimal effects on the DOX release from the **Fe_3O_4@SiO_2@meso-SiO_2@NH_2** NPs were observed. It is reasonable to conclude that the crown ethers play an important role as nanogate to control the DOX release.

dx.doi.org/10.1021/am4004705 | ACS Appl. Mater. Interfaces 2013, 5, 1566−1574

Table 1. Summary of Percentage of Drug Loading for 200 μg of Different NPs and 250 μg/mL of DOX

nanoparticle	% drug loading			
	H_2O	1 M HCl	1 M CsCl	1 M NaCl
Fe_3O_4@SiO_2@meso-SiO_2-NH_2	31 ± 9	2 ± 1	3 ± 2	8 ± 6
Fe_3O_4@SiO_2@meso-SiO_2@crown ether(1a)	55 ± 6	8 ± 6	16 ± 6	18 ± 12
Fe_3O_4@SiO_2@meso-SiO_2@crown ether(1b)	43 ± 1	9 ± 3	1 ± 1	32 ± 6
Fe_3O_4@SiO_2@meso-SiO_2@crown ether(1c)	47 ± 1	2 ± 1	5 ± 3	23 ± 1

Table 2. Binding Constants Determined by Isothermal Titration Calorimetry in MeCN/H_2O (9:1)

crown ether	binding constant (× 10^5 M^{-1}) with different ions	
	Na^+	Cs^+
1a	1.31	1.33
1b	1.27	1.30
1c	1.25	1.29

For the case of **Fe_3O_4@SiO_2@meso-SiO_2@crown ether(1a)**, only in the presence of ultrasound and Na^+ ions at pH 4 was there a dramatic 10% increase in releasing DOX drug molecules from the NP. After the ultrasound-triggered release, the nanoparticle was subjected to TGA once again. The TGA result revealed nearly the same % organic fraction loss which demonstrated that the corwn ethers were still intact with the nanoparticle. On the other hand, the binding constants of different crown ethers (**1a–c**) with Na^+ or Cs^+ have been determined, in the range of 1 × 10^5 M^{-1} (Table 2). The mechanism by using the crown ether-containing NP systems can be postulated. It has been reported that ultrasound wave would induce phase separation between hydrophobic and salt-containing hydrophilic layers.[43−45] In our study, therefore, it is envisaged that more than one Na^+ ion will bind to the peripheral environment of crown ether **1a** (**1a**⊃xNa^+) by electrostatic interaction to block the pores without leaking of DOX. When ultrasound is applied to the NP, the bound Na^+ ions will gradually solvate into the solution and rapidly replace and stabilize by H^+ with a competitive binding toward the crown ether. The smaller crown ether-proton complexes (**1a**⊃xH^+) will no longer act as blockers for the nanogate and as a result, a release of DOX molecules is triggered. On the other hand, it is envisaged that a Cs^+ ion will bind to the crown ether **1a** (**1a**⊃Cs^+) by electrostatic interaction to block the pores without leaking of DOX. Because the **1a**⊃Cs^+ complex is more stable with preorganized structure and multiple supramolecular interactions, the use of ultrasound with the same intensity to solvate the Cs^+ becomes less effective. Therefore, this **1a**⊃Cs^+ structure can act as a block for the pores.

Therefore, the DOX triggering event inevitably requires metal cations, protons (acidic pH), and ultrasound. The use of larger crown ethers (**1b** and **1c**) possess similar triggering event with multivalent binding of Na^+ toward the crown ethers at pH 4 with ultrasound. However, Cs^+ ions may not be best fitted to the enlarged crown ethers with a slight decrese in their binding constants so that **1b**⊃Cs^+ or **1c**⊃Cs^+ complexes are not effective blockers anymore. With ultrasound application, the DOX molecules release out from the pore because either Cs^+ ions may solvate or DOX molecules may gain enough energy to escape from a leaking nanogate.

MR relaxometry of functionalized NPs was performed using a clinical 1.5 T whole body MR system in combination with a knee radio frequency coil for excitation and signal reception. The MRI results of the functionalized NPs are shown in Figure S19 in the Supporting Information. The MRI relaxivity r_2,

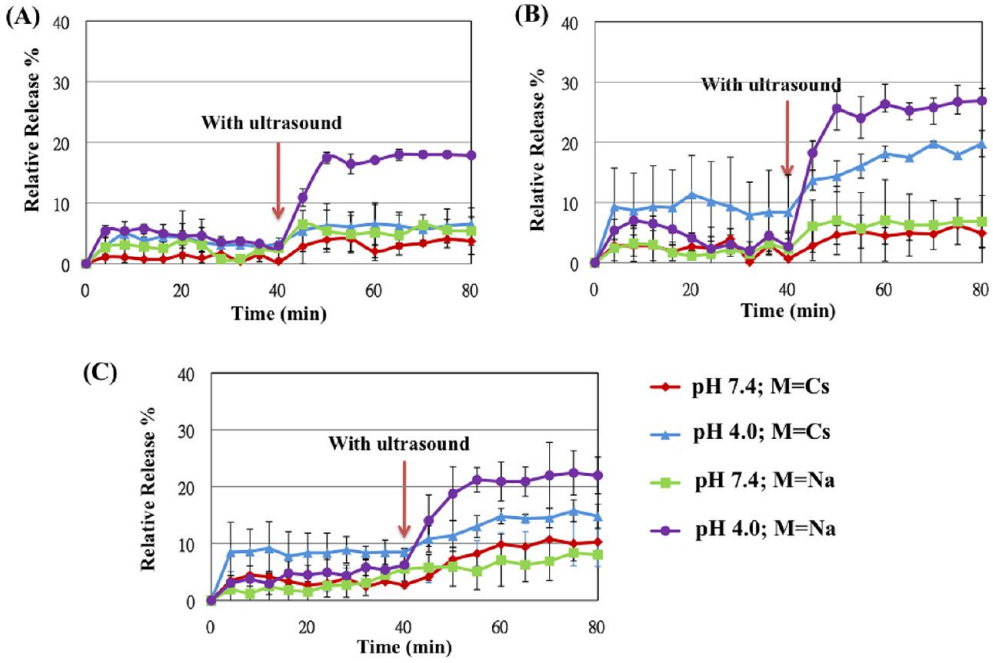

Figure 7. DOX drug release profiles from NPs in PBS at 298 K triggered by ultrasound application (monitored at 490 nm). (A) **Fe_3O_4@SiO_2@meso(DOX)-SiO_2@crown ether(1a)**⊃M^+, (B) **Fe_3O_4@SiO_2@meso(DOX)-SiO_2@crown ether(1b)**⊃M^+, and (C) **Fe_3O_4@SiO_2@meso(DOX)-SiO_2@crown ether(1c)**⊃M^+.

dx.doi.org/10.1021/am4004705 | ACS Appl. Mater. Interfaces 2013, 5, 1566−1574

which is a measure of the change in spin−spin relaxation rate (T_2^{-1}) per unit iron concentration, was determined as 103.5 ± 4.7, 162.7 ± 8.0, and 137.6 ± 9.2 mM^{-1} s^{-1} for **Fe_3O_4@SiO_2@meso-SiO_2@crown ether(1a)**, **Fe_3O_4@SiO_2@meso-SiO_2@crown ether(1b)**, and **Fe_3O_4@SiO_2@meso-SiO_2@crown ether(1c)**, respectively. As expected for T_2 contrast agents, the signal dark intensity of the in vitro MR images (Figure 8)

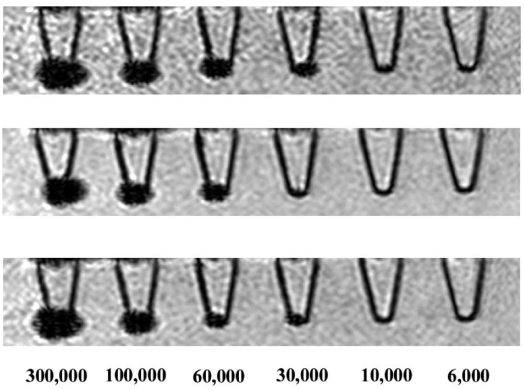

Figure 8. In vitro MRI results of functionalized NPs with different cell numbers. Fe_3O_4@SiO_2@meso-SiO_2@crown ether(1a) (top), Fe_3O_4@SiO_2@meso-SiO_2@crown ether(1b) (middle), and Fe_3O_4@SiO_2@meso-SiO_2@crown ether(1c) (bottom).

increases when superparamagnetic NP concentration increases. **Fe_3O_4@SiO_2@meso-SiO_2@crown ether(1a)** and **Fe_3O_4@SiO_2@meso-SiO_2@crown ether(1c)** possessed better cell labeling efficacies, whereas MR signal for 6000 cells are observable. These MR results echo to the cell labeling experiments described above (Figure 6).

4. CONCLUSION

A series of novel dibenzo-crown ethers **1a−c** were coupled to form core@shell **Fe_3O_4@SiO_2@meso-SiO_2@crown ether(1a-c)** NPs and characterized by TEM, EDX, IR and TGA. The biological study of the theranostic NPs was investigated and confirmed that they are biocompatible and relatively non-cytotoxic toward L929 cells. In addition, cellular uptake of these NPs in L929 cells was determined with reasonable uptake of NPs, ranging from 1.7×10^{-5} to 2.3×10^{-5} μg/cell. Also, the MR relaxivities of these NPs were ranging from 104 to 163 mM^{-1} s^{-1} determined by clinical 1.5 T whole body MR system. Moreover, the effect of stimuli toward doxorubicin drug loading was investigated. It indicated that the crown ether-based nanovalves on the surface of NPs could be blocked by Cs^+ and Na^+ ions and possessed of different modes of drug loading and release. Drug loading could be effectively facilitated in water at neutral pH in the absence of metal ions. Most importantly, the release profiles of DOX molecules from the NPs were enhanced and triggered by ultrasound for the Na^+-treated **Fe_3O_4@SiO_2@meso(DOX)-SiO_2@crown ether(1a-c)⊃Na^+** NP systems. These results suggested that the release of drug molecules from NPs with crown ether-based nanovalves with metal cation blocking could be triggered by lowering the pH and in the presence of ultrasound, breaking up the electrostatic interaction between metal cations and crown ether's ethylene glycol chains. In summary, the novel controlled release systems by the use of dibenzo-crown ethers as nanovalves were successfully demonstrated and found that the release of drug could be triggered at pH 4 in the presence of noninvasive ultrasound, wherein these noncytotoxic NP systems are potentially used for ultrasound-based biomedical applications for general cancer theranostic purposes.[46]

■ ASSOCIATED CONTENT

Ⓢ Supporting Information

Detailed synthesis of crown ethers, additional TEM images, additional drug loading and release data, NMR, FTIR, EDX, TGA, and UV/visible absorption spectra. This material is available free of charge via the Internet at http://pubs.acs.org.

■ AUTHOR INFORMATION

Corresponding Author

*Phone: (+852) 3411 2319. E-mail: cfleung@hkbu.edu.hk.

Notes

The authors declare no competing financial interest.

■ ACKNOWLEDGMENTS

This work was supported by General Research Fund schemes (401808 and 401709) from The Research Grants Council of Hong Kong, HKBU-FRG (FRG1/11-12/031) and AoE/P-03/08 research grants.

■ REFERENCES

(1) Li, Z.; Barnes, J. C.; Bosoy, A.; Stoddart, J. F.; Zink, J. I. *Chem. Soc. Rev.* **2012**, *41*, 2590−2605.
(2) Vallet-Regí, M.; Balas, F.; Arcos, D. *Angew. Chem., Int. Ed.* **2007**, *46*, 7548−7558.
(3) Tang, F.; Li, L.; Chen, D. *Adv. Mater.* **2012**, *24*, 1504−1534.
(4) Yang, P.; Gai, S.; Lin, J. *Chem. Soc. Rev.* **2012**, *41*, 3679−3698.
(5) Leung, K. C.-F.; Xuan, S. H.; Zhu, X. M.; Wang, D. W.; Chak, C.-P.; Lee, S.-F.; Ho, W. K.-W.; Chung, B. C.-T. *Chem. Soc. Rev.* **2012**, *41*, 1911−1928.
(6) Radu, D. R.; Lai, C.-Y.; Jeftinija, K.; Rowe, E. W.; Jeftinja, S.; Lin, V. S.-Y. *J. Am. Chem. Soc.* **2004**, *126*, 13216−13217.
(7) Liong, M.; Lu, J.; Kovochich, M.; Xia, T.; Ruehm, S. G.; Nel, A. E.; Tamanoi, F.; Zink, J. I. *ACS Nano* **2008**, *2*, 889−896.
(8) Zhu, Y.; Ikoma, T.; Hanagata, N.; Kaskel, S. *Small* **2010**, *6*, 471−478.
(9) Choi, Y. L.; Jaworski, J.; Seo, M. L.; Lee, S. J.; Jung, J. H. *J. Mater. Chem.* **2011**, *21*, 7882−7885.
(10) Knezevic, N. Z.; Slowing, I. I.; Lin, V. S.-Y. *ChemPlusChem* **2012**, *77*, 48−55.
(11) Chen, X.; Gambhir, S. S.; Cheon, J. *Acc. Chem. Res.* **2011**, *10*, 841−841.
(12) Yang, X.; Grailer, J. J.; Rowland, I. J.; Javadi, A.; Hurley, S. A.; Matson, V. Z.; Steeber, D. A.; Gong, S. *ACS Nano* **2010**, *4*, 6805−6817.
(13) Ke, H.; Wang, J.; Dai, Z.; Jin, Y.; Qu, E.; Xing, Z.; Guo, C.; Yue, X.; Liu, J. *Angew. Chem., Int. Ed.* **2011**, *50*, 3017−3021.
(14) Husseini, G. A.; Pitt, W. G. *Adv. Drug Delivery Rev.* **2008**, *60*, 1137−1152.
(15) Rapoport, N.; Kennedy, A. M.; Shea, J. E.; Scaife, C. L.; Nam, K.-H. *Mol. Pharm.s* **2010**, *7*, 22−31.
(16) Wang, Y.-X. J.; Leung, K. C.-F.; Cheung, W.-H.; Wang, H.-H.; Shi, L.; Wang, D.-F.; Qin, L.; Ahuja, A. T. *J. Magn. Resonance Imaging* **2010**, *31*, 1508−1513.
(17) Soman, N. R.; Marsh, J. N.; Lanza, G. M.; Wickline, S. A. *Nanotechnology* **2008**, *19*, 185102.
(18) Chen, D.; Wu, J. *Ultrasonics* **2010**, *50*, 744−749.
(19) Liu, T.-Y.; Huang, T. C. *Acta Biomater.* **2011**, *7*, 3927−3934.
(20) Wang, C.-Y.; Yang, C.-H.; Lin, Y.-S.; Chen, C.-H.; Huang, K.-S. *Biomaterials* **2012**, *33*, 1547−1553.
(21) Harada, A.; Ono, M.; Yuba, E.; Kono, K. *Biomater. Sci.* **2013**, *1*, 65−73.

(22) Harada, Y.; Ogawa, K.; Irie, Y.; Endo, H.; Feril, L. B., Jr.; Uemura, T.; Tachibana, K. *J. Controlled Release* **2011**, *149*, 190−195.
(23) Ambrogio, M. W.; Thomas, C. R.; Zhao, Y.-L.; Zink, J. I.; Stoddart, J. F. *Acc. Chem. Res.* **2011**, *44*, 903−913.
(24) Yang, Y.-W. *MedChemComm* **2011**, *2*, 1033−1049.
(25) Gokel, G. W.; Leevy, W. M.; Weber, M. E. *Chem. Rev.* **2004**, *104*, 2723−2750.
(26) Zhu, X.-M.; Yuan, J.; Leung, K. C.-F.; Lee, S.-F.; Sham, K. W. Y.; Cheng, C. H. K.; Au, D. W. T.; Teng, G.-J.; Ahuja, A. T.; Wang, Y.-X. J. *Nanoscale* **2012**, *4*, 5744−5754.
(27) Nguyen, T. D.; Liu, Y.; Saha, S.; Leung, K. C.-F.; Stoddart, J. F.; Zink, J. I. *J. Am. Chem. Soc.* **2007**, *129*, 626−634.
(28) Deng, Y.; Qi, D.; Deng, C.; Zhang, X.; Zhao, D. *J. Am. Chem. Soc.* **2008**, *130*, 28−29.
(29) Xuan, S. H.; Lee, S.-F.; Lau, J. T.-F.; Zhu, X.; Wang, Y.-X. J.; Wang, F.; Lai, J. M. Y.; Sham, K. W. Y.; Lo, P. C.; Yu, J. C.; Cheng, C. H. K.; Leung, K. C.-F. *ACS Appl. Mater. Interfaces* **2012**, *4*, 2033−2040.
(30) Leung, K. C.-F.; Chak, C.-P.; Lo, C.-M.; Wong, W.-Y.; Xuan, S. H.; Cheng, C. H. K. *Chem. Asian J.* **2009**, *4*, 364−381.
(31) Suslick, K. S.; Price, G. J. *Annu. Rev. Mater. Sci.* **1999**, *29*, 295−326.
(32) Wu, Z.; Ondruschka, B.; Stark, A. *J. Phys. Chem. A* **2005**, *109*, 3762−3766.
(33) Cai, Y.; Pan, H.; Xu, X.; Hu, Q.; Li, L.; Tang, R. *Chem. Mater.* **2007**, *19*, 3081−3083.
(34) Kwon, E. J.; Lee, T. G. *Appl. Surf. Sci.* **2008**, *254*, 4732−4737.
(35) Ke, H.; Wang, J.; Dai, Z.; Jin, Y.; Qu, E.; Xing, Z.; Guo, C.; Yue, X.; Liu, J. *Angew. Chem., Int. Ed.* **2011**, *50*, 3017−3021.
(36) Chong, A. S. M.; Zhao, X. S. *J. Phys. Chem. B* **2003**, *107*, 12650−12657.
(37) Nakazawa, J.; Stack, T. D. P. *J. Am. Chem. Soc.* **2008**, *130*, 14360−14361.
(38) Lin, V. S.-Y.; Radu, D. R.; Han, M.-K.; Deng, W.; Kuroki, S.; Shanks, B. H.; Pruski, M. *J. Am. Chem. Soc.* **2002**, *124*, 9040−9041.
(39) Lai, C.-Y.; Trewyn, B. G.; Jeftinija, D. M.; Jeftinija, K.; Xu, S.; Jeftinija, S.; Lin, V. S.-Y. *J. Am. Chem. Soc.* **2003**, *125*, 4451−4459.
(40) Zhu, X.-M.; Wang, Y.-X. J.; Leung, K. C.-F.; Lee, S.-F.; Zhao, F.; Wang, D.-W.; Lai, J. M. Y.; Wan, C.; Cheng, C. H. K.; Ahuja, A. T. *Int. J. Nanomed.* **2012**, *7*, 953−964.
(41) Chang, B.; Guo, J.; Liu, C.; Qian, J.; Yang, W. *J. Mater. Chem.* **2010**, *20*, 9941−9947.
(42) Leung, K. C.-F.; Nguyen, T. D.; Stoddart, J. F.; Zink, J. I. *Chem. Mater.* **2006**, *18*, 5919−5928.
(43) Seymour, J. D.; Gupta, R. B. *Ind. Eng. Chem. Res.* **1997**, *36*, 3453−3457.
(44) Bardelang, D.; Zaman, M. B.; Moudrakovski, I. L.; Pawsey, S.; Margeson, J. C.; Wang, D.; Wu, X.; Ripmeester, J. A.; Ratcliffe, C. I.; Yu, K. *Adv. Mater.* **2008**, *20*, 4517−4520.
(45) Chaudhary, D.; Liu, H. *Ultrason. Sonochem.* **2013**, *20*, 63−68.
(46) Kaneko, O. F.; Willmann, J. K. *Quant. Imaging Med. Surg.* **2012**, *2*, 87−97.